THE JOURNAL OF PHYSICAL CHEMISTRY C

Article

pubs.acs.org/JPCC

Influence of Blend Ratio and Processing Additive on Free Carrier Yield and Mobility in PTB7:$PC_{71}BM$ Photovoltaic Solar Cells

Vytenis Pranculis,[†] Arvydas Ruseckas,[‡] Dimali A. Vithanage,[‡] Gordon J. Hedley,[‡] Ifor D. W. Samuel,*[,‡] and Vidmantas Gulbinas*[,†]

[†]Center for Physical Sciences and Technology, Savanoriu Ave 231, 02300 Vilnius, Lithuania

[‡]Organic Semiconductor Centre, SUPA, School of Physics and Astronomy, University of St. Andrews, St. Andrews KY16 9SS, United Kingdom

ABSTRACT: Charge separation and extraction dynamics were investigated in high-performance bulk heterojunction solar cells made from the polymer PTB7 and the soluble fullerene $PC_{71}BM$ on a broad time scale from subpicosecond to microseconds using ultrafast optical probing of carrier drift and the integral-mode photocurrent measurements. We show that the short circuit current is determined by the separation of charge pairs into free carriers, which is strongly influenced by blend composition. This separation is found to be efficient in fullerene-rich blends where a high electron mobility of >0.1 $cm^2\ V^{-1}\ s^{-1}$ is observed in the first 10 ps after excitation. Morphology optimization using the solvent additive 1,8-diiodooctane (DIO) doubles the charge pair separation efficiency and the short-circuit current. Carrier extraction at low internal electric field is slightly faster from the cells prepared with DIO, which can reduce recombination losses and enhance a fill factor.

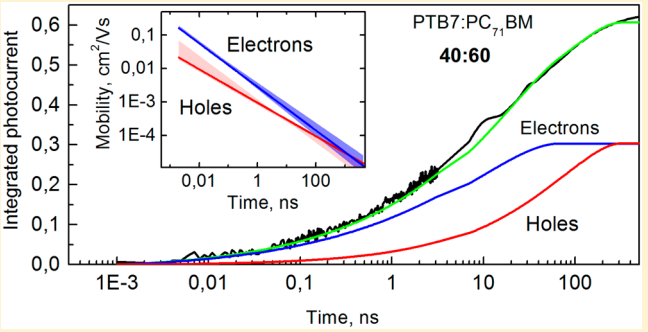

INTRODUCTION

The limited supply of fossil fuels and rising energy demands have encouraged research into renewable energy sources, with photovoltaics proving to be a suitable candidate. Interest in organic and hybrid solar cells has grown due to their ability to produce flexible lightweight devices with low manufacturing costs and an abundant supply of environmentally friendly materials. Small-scale single-junction organic solar cells now achieve power conversion efficiencies over 10%.[1−4] The best performance is achieved using a bulk heterojunction where an electron donor (usually a conjugated polymer) and an acceptor (usually a fullerene) are blended to obtain a large interfacial area for charge carrier generation. Progress has been spurred on by the synthesis of novel polymers and optimization of processing conditions. One of the most efficient blends is of the polymer PTB7 and the soluble fullerene $PC_{71}BM$, and it achieves high efficiency using a high-boiling-point solvent additive 1,8-di-iodooctane (DIO) for processing the active layer.[4−9] The influence of DIO on the morphology of PTB7:$PC_{71}BM$ blends has previously been investigated in detail, which indicated that the blends prepared without additive show pure fullerene clusters of 20−60 nm in size which form large agglomerates embedded in a polymer-rich matrix containing about 30 wt % of fullerene.[10−13] The addition of DIO to the casting solvent improves the miscibility of $PC_{71}BM$ with PTB7, dramatically shrinks the size of the clusters to several nanometers, and forms interpenetrating polymer-rich and fullerene-rich phases of tens of nanometers in size.[10,12] Fluorescence quenching was found to be of similar efficiency in blends prepared with additive and without, suggesting that the increase of power conversion efficiency is not due to more efficient charge generation.[12] This is consistent with the power conversion efficiency enhancements occurring in both the polymer and fullerene absorption regions, suggesting that the improvement results from reduced carrier recombination.[10,12] The origin of reduced recombination is not known; possible explanations include improved charge separation, higher carrier mobility, or reduced charge trapping.[12,14−16] It is therefore clear that a detailed understanding of the free carrier generation, transport, and extraction in this important high-performance blend is lacking.

In this work, we combine transient photocurrent measurements with ultrafast optical probes of carrier mobility to investigate charge separation and motion dynamics in PTB7:$PC_{71}BM$ solar cells in order to understand the reasons behind the increased efficiency of devices prepared with the additive DIO. We demonstrate that the increase of photocurrent in devices prepared with DIO occurs because of a higher dissociation efficiency of photogenerated charge pairs into free carriers. The enhancement of the carrier extraction rate is observed at a low built-in electric field and can contribute to a higher fill factor of DIO-prepared solar cells. We measured time-dependent carrier mobility in devices prepared using different blending ratios and show that carrier transport is

Received: February 15, 2016
Revised: April 21, 2016
Published: April 22, 2016

DOI: 10.1021/acs.jpcc.6b01548
J. Phys. Chem. C 2016, 120, 9588−9594

limited by connectivity of fullerene/polymer domains in addition to trapping at low energy sites. These results give new insights into the influence of morphology on charge separation and transport, providing a full picture of the dynamics of these processes helping to understand the operation mechanisms and the ways to improve the performance.

EXPERIMENTAL METHODS

Solar Cell Preparation and Characterization. PTB7 with a molecular weight of 92000 and a polydispersity of 2.6 was obtained from 1-Material, Inc. $PC_{71}BM$ of 99% purity was obtained from Solenne and DIO from Sigma-Aldrich. PTB7 and fullerene were dissolved in chlorobenzene (HPLC grade from Sigma-Aldrich) at ratios of 90:10, 40:60, 20:80, and 10:90 by weight and stirred at 50 °C for 4−5 h. We will call these blends [P90:F10], [P40:F60], [P20:F80], and [P10:F90], respectively, where the first number denotes the relative amount of the polymer. For the samples prepared with DIO, 3% of it by volume was added to the solution which was then stirred for a further 5 min. The blends were spin-coated on a ∼40 nm layer of PEDOT:PSS which was spin-coated on an indium−tin oxide coated glass substrate. The thickness of the PTB7:fullerene layer was ∼115 nm. The layers of calcium (∼20 nm) and aluminum (∼100 nm) were subsequently deposited by vacuum sublimation. The structure was encapsulated with a glass coverslip and epoxy. The current−voltage characteristics were measured under AM1.5 conditions using a solar simulator from Sciencetech and the intensity calibrated with an ORIEL reference cell with KG5 filter. The spectral mismatch factor was close to unity (0.995) for PTB7:$PC_{71}BM$. An aperture of the same size as the pixel was used to avoid contribution from stray light outside the device area.

Measurements of Carrier Drift Dynamics. To measure the carrier-drift dynamics, we have used the time-resolved electric-field-induced second-harmonic generation (TREFISH) technique, which was described in detail elsewhere.[17] Briefly, a pulsed p-polarized probe light is shone on a cell at ∼45° incidence angle. An applied electric field F breaks centrosymmetry of the blend for incident light so that the second harmonic of the probe light (SH) is generated and its intensity is proportional to F^2. An optical pump pulse which overlaps spatially with the probe light generates charge pairs which drift in response to electric field, and so they shield the internal electric field and reduce the SH intensity. In this way, the intensity of SH can be used to directly monitor carrier drift in the cell by changing the time delay between pump and probe pulses. The solar cell acts as a parallel plate capacitor; thus, $F = (U_{appl} + \Delta W/e)/L$ where U_{appl} is the applied reverse bias, $\Delta W = -0.8$ eV is the difference of work functions of the electrodes, L is the distance between the electrodes, and e is the elementary charge. The SH dependence on the applied voltage without a pump pulse was measured first and used later to obtain the strength of the internal electric field from the TREFISH signal. Probe pulses at 800 nm and 1 kHz repetition rate were generated by a regenerative amplifier (Quantronix Integra-C), and SH was detected using a photomultiplier tube. The pump pulses were generated in an optical parametric amplifier TOPAS-C (Light Conversion) and excited the cell at 500 Hz, i.e., at every other probe pulse. The pump wavelength was 680 nm, which is the absorption maximum of the polymer. Pump and probe pulses were 150 fs long. The integral-mode photocurrent transients were measured simultaneously using the same pump pulses and recording the voltage on a 10 kΩ load resistor connected in series with the solar cell using a 500 MHz bandwidth Agilent Technologies oscilloscope DSO5054A. The pump pulse energy was adjusted to give photocurrent transients which were independent of pump energy, indicating negligible nongeminate recombination of charge pairs. The measurements were performed using pump pulse energy densities of 80, 120, 160, and 500 nJ cm^{-2} in the solar cells prepared with the PTB7:$PC_{71}BM$ blending ratios of 40:60, 20:80, 10:90, and 90:10 by weight, respectively.

RESULTS

Photovoltaic Response. Figure 1 shows the current−voltage characteristics of the solar cells at the optimum blend ratio [P40:F60], prepared with and without DIO measured under AM1.5 illumination conditions. The device prepared with DIO shows about two times higher short-circuit current (J_{sc}) and fill factor (FF). The open circuit voltage (V_{oc}) does not depend on the solvent additive. The power conversion efficiency (PCE) of the device prepared with DIO was 5.4% at AM1.5 conditions. It is important to note that our device stack has identical active layer properties (blend ratio, solution concentration, spin-coating deposition parameters, thickness, deposition onto PEDOT) as the best reported devices but suffers from lower overall performance owing to nonoptimized contacts, giving us efficiencies comparable to those which others report with similar nonoptimized contacts.[5,10,12] Nonetheless, we still see the same dramatic improvement in overall device performance with the addition of DIO and can use this as a basis for understanding in this article how the changes in morphology that are known to be occurring influence the electronic properties of the device.

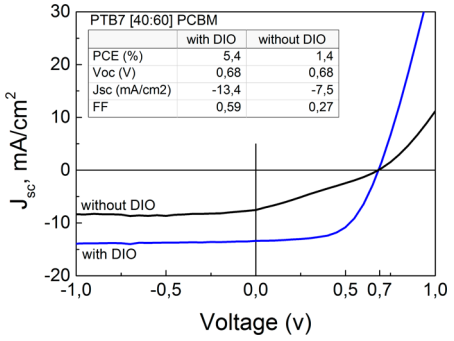

Figure 1. Current−voltage characteristics of the PTB7:$PC_{71}BM$ [40:60] solar cells under 1 Sun illumination.

Charge Separation and Extraction Dynamics in Optimized Cells. Figure 2 shows the photoinduced voltage drop ΔU in the devices with 60 wt % of $PC_{71}BM$ which have the highest power conversion efficiency. It is measured by TREFISH in the time range from 0 to 3 ns using $\Delta U = \Delta F(t)L$ where $\Delta F(t)$ is a decrease of the electric field strength due to carrier displacement and L is the sample thickness. The long-time data are obtained from the integral-mode photocurrent. The combination of the two techniques enables us to monitor carrier drift kinetics from subpicoseconds to tens of microseconds, starting from their photogeneration up to extraction from the devices. The photoinduced voltage drop is proportional to the amount of extracted charge in a time interval t

DOI: 10.1021/acs.jpcc.6b01548
J. Phys. Chem. C 2016, 120, 9588−9594

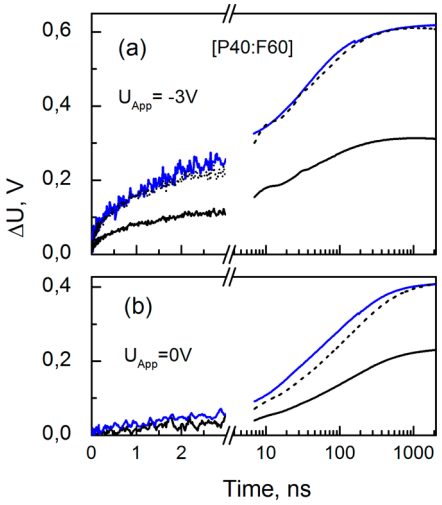

Figure 2. Photoinduced voltage drop in devices with 60 wt % of $PC_{71}BM$ at 3 V reverse bias (a) and at the built-in field only (b) as a function of time after the pump pulse. The results are derived from TREFISH measurements up to 3 ns and from the integral-mode photocurrent at longer times (note log scale after the axis break). Black curves correspond to devices without DIO, blue to devices with DIO. Black dotted curves show the kinetics from devices without DIO which are scaled to match the voltage drop in devices with DIO at late times. Pump density was 4×10^{11} absorbed photons/cm^2 at the peak of polymer absorption (680 nm).

$$\Delta U(t) = \frac{1}{C}\int_0^t I(t')\,dt' \quad (1)$$

where C is the sample capacitance and $I(t)$ is photocurrent. The voltage drop at long times is proportional to the total amount of extracted charge from the device. At 1000 ns, it is two times bigger in devices prepared with DIO, which agrees well with the approximately two times higher photocurrent observed in current−voltage characteristics at the short-circuit condition and at reverse bias (Figure 1). In order to more clearly compare the extraction kinetics, Figure 2 presents the voltage kinetics for the sample without DIO normalized to that for the sample with DIO. They show that charge extraction at the 3 V bias is only marginally faster from the cell prepared with DIO. The difference is slightly stronger at 0 V bias. This indicates that the extraction efficiency of free carriers with a strong internal field is not particularly sensitive to morphology and suggests that the increased short circuit photocurrent in devices prepared with DIO is mainly due to more efficient charge separation rather than extraction. Combining this with previous observations that the charge generation efficiency is similar in blends prepared with additive and without,[12] we conclude that the increase of photocurrent in devices prepared with DIO occurs mainly because of a higher dissociation efficiency of photogenerated charge pairs. The charge extraction at 0 V bias is faster in a device prepared with DIO as the time taken to extract a half of the charge decreases from 60 ns without DIO to 40 ns with DIO. In this case, the internal electric field in the cell is lower than at the short circuit condition because the total voltage drop on the load resistor comes to nearly a half of the built-in voltage. A faster charge extraction from DIO-prepared devices at low built-in field reduces recombination losses and can explain the higher fill factor of solar cells prepared with DIO.

Influence of Internal Electric Field. In order to explore the influence of electric field, blend ratio, and the use of DIO on the charge separation efficiency, we studied the dependence of the amount of extracted charge in 1 μs on the applied external voltage (Figure 3). The amount of extracted charge

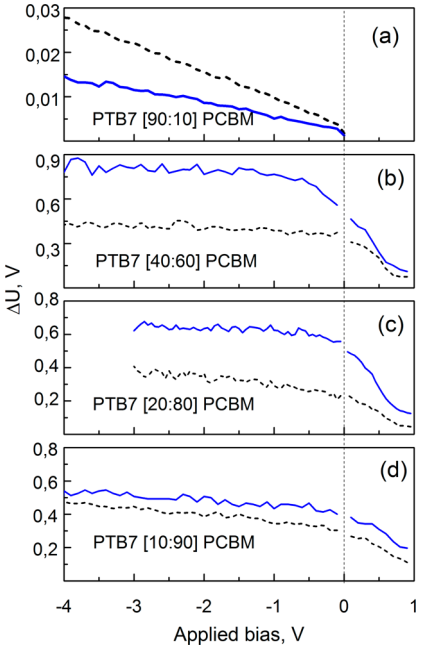

Figure 3. Photoinduced voltage drop at 1 μs from the integral-mode photocurrent measurements vs an applied external voltage in devices with different blend ratios for the excitation density of 4×10^{11} absorbed photons/cm^2. Dotted black and blue curves correspond to the devices without and with DIO, respectively.

from the cell with 10 wt % fullerene shows approximately linear dependence on the reverse bias with no saturation even at −4 V. At its maximum, ΔU from this cell is still about 20 times lower than from the cells with high fullerene content. This indicates that in the blend with low fullerene content the charge pairs are strongly bound and can only be separated by strong electric fields. It is interesting to note that the additive DIO decreases the amount of extracted charge from the polymer-rich blend, which is opposite to what is observed in the fullerene-rich blends, and the reduction factor is independent of the applied bias. In contrast, the amount of charge extracted from other three blends is much higher and shows a weak dependence on the bias between −1 and −4 V indicating that a weaker electric field is sufficient to drive charge separation in fullerene-rich blends. This result is consistent with previous observations of efficient free carrier generation in fullerene-rich blends[18,19] and much higher initial electron mobility in the fullerene than the hole mobility in the electron donors observed by means of THz spectroscopy.[20] The amount of charge extracted from the blends with 80 and 90 wt % fullerene increases by about 30% with the increase of the negative bias between −1 and −4 V (Figure 3 c,d). We attribute this to carrier generation from excitons deep inside $PC_{71}BM$ domains, a process which is assisted by an electric field. At high $PC_{71}BM$ concentrations the absorption by fullerene at the excitation wavelength (680 nm) is comparable to that of the polymer and many excitons are generated deep inside the fullerene phase. The three-dimensional exciton diffusion length in $PC_{71}BM$ can be estimated as $\sqrt{6D\tau}$ where D is exciton diffusivity and τ is the exciton lifetime. Using the reported D and τ values,[12] we

DOI: 10.1021/acs.jpcc.6b01548
J. Phys. Chem. C 2016, 120, 9588−9594

estimate the exciton diffusion length of about 7 nm in the bulk $PC_{71}BM$. With polymer concentrations at only 10−20 wt % not all excitons created in fullerene domains reach the heterojunction. Charge carriers can be generated inside the fullerene domains with the assistance of an electric field as observed previously[21,22] which can explain why the free carrier yield is bias-dependent. This suggests that carrier generation mechanism in the fullerene-rich blends could be different, depending if photon is absorbed by the polymer or by $PC_{71}BM$.

Effect of Blend Ratio and Solvent Additive on Carrier Mobility. In order to understand the role of electron and hole motion in charge separation and the effect of morphology we studied the time-dependence of carrier extraction from devices prepared with different blend ratios (Figure 4). The blends with

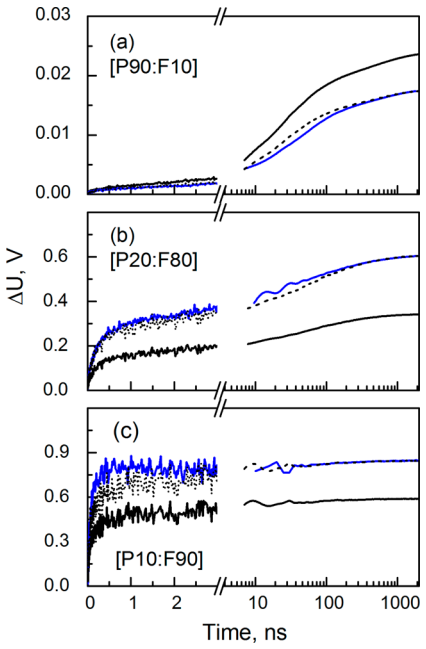

Figure 4. Photoinduced voltage drop for the pump density of 4×10^{11} absorbed photons/cm^2 in PTB7:$PC_{71}BM$ devices with very low and high fullerene content at 3 V reverse bias. Black curves correspond to devices without DIO, blue to devices with DIO. Black dotted curves show the kinetics from devices without DIO which are scaled to match the voltage drop in devices with DIO at long times.

high fullerene content show an enhancement of the amount of extracted charge when prepared with DIO. The enhancement factor is slightly lower than that observed in a blend with 60 wt % fullerene (Figure 2). All fullerene-rich blends show a fast extraction phase within 10 ns which is followed by a slow phase on the 10−100 ns time scale. The fast phase gets faster with increasing fullerene content. In the blend with 60 wt % fullerene a half of the mobile carriers are extracted in ∼10 ns at a 3 V reverse bias (Figure 2a), whereas in the blend with 80 wt % fullerene this happens in ∼2 ns (Figure 4b). Even faster carrier extraction is observed in the blend with 90 wt % fullerene, which is complete in ∼0.5 ns. This is similar to previous observations of very fast electron extraction from neat $PC_{61}BM$ films.[21] In contrast, carrier extraction from the polymer-rich blend is much slower and occurs on a 100−1000 ns time scale. This trend allows us to assign the fast extraction phase in fullerene-rich blends to electrons and the slow phase to holes. The additive DIO enhances the electron extraction rate from the fullerene-rich blends, but slightly slows down carrier extraction from the polymer-rich blend.

In order to evaluate the electron and hole mobilities and their dependence on the blend ratio, we have fitted the photoinduced voltage drop to a sum of integrated electron and hole photocurrents

$$\Delta U(t) = -\frac{eFA}{C}\int_0^t [N_e\mu_e(t') + N_h\mu_h(t')]\,dt' \quad (2)$$

Here, e is the electron and hole charge, F is the electric field strength, A is the area illuminated by the pump pulse, C is the cell capacitance, $N_{e,h}(t) = N_0(1 - \langle\chi_{e,h}(t)\rangle/L)$ are the average electron and hole concentrations in the cell with an account for carrier extraction, $\mu_{e,h}$ are their mobilities, N_0 is the density of generated charge pairs, and $\langle\chi_e(t)\rangle$ and $\langle\chi_h(t)\rangle$ are the average electron and hole drift distances $\langle\chi_{e,h}(t)\rangle = F\int_0^t\mu_{e,h}(t)\,dt$. The model assumes homogeneous carrier generation within the sample thickness. We approximated the electron and hole mobilities by functions $\mu_{e,h}(t) = \mu_{0e,h}t^{-\alpha}$ to account for their time dependences. A similar modeling procedure has been used in ref 18. Because of very low excitation densities, the losses to nongeminate carrier recombination are negligible. Figure 5 presents the fits to the voltage kinetics for blends without DIO as well as the electron and hole contributions to it. The simulations reproduce the experimental results well for the [P40:F60] and [P20:F80] samples, while the fits for the two

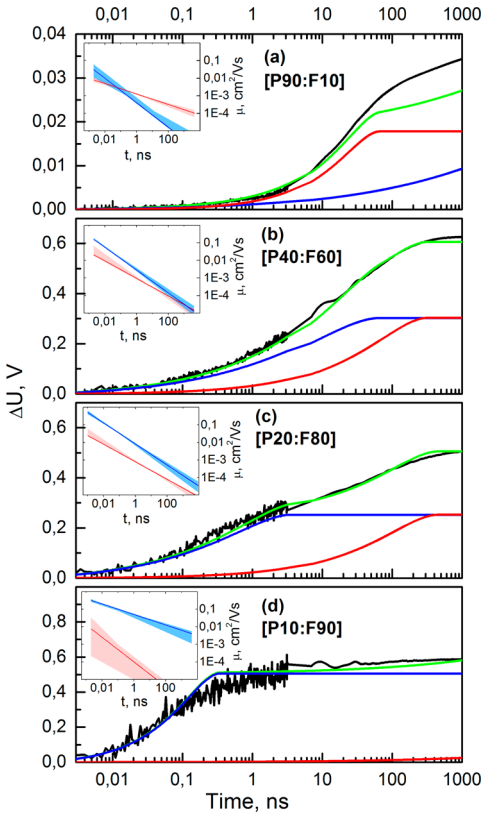

Figure 5. Modeling results of the carrier extraction kinetics from the cells prepared with different blend ratios without DIO at 3 V reverse bias. Black lines are the experimental data, green lines are the modeled kinetics, blue and red lines show electron and hole contributions, respectively. Insets show time-dependent electron (blue lines) and hole (red lines) mobility obtained from the fits. Shadows show the estimated error ranges.

DOI: 10.1021/acs.jpcc.6b01548
J. Phys. Chem. C 2016, 120, 9588−9594

extreme blend ratios are much worse. It is apparent that the power law functions cannot adequately describe the time dependences of the carrier mobilities at very low donor or acceptor concentrations. This is not surprising because these concentrations are at the percolation limit, and one type of carriers will inevitably encounter dead ends of charge transporting domains.[23] As Figures 2 and 4 show, normalized carrier motion dynamics in blends with and without DIO are very similar, giving very similar mobility values and kinetics; therefore, they are not presented and we will not specify it in discussion. The simulated electron and hole contributions to integrated current show that just about 50% of electrons are extracted in 1 μs from the blend with 10 wt % of fullerene (Figure 5a) and only about 2% of holes from the blend with 90 wt % of fullerene (Figure 5d). This indicates that the extraction of the rest of carriers takes much longer time than 1 μs in these blends with extreme ratios; thus, carrier extraction is strongly unbalanced. In solar cells with the optimal blend ratio of 60 wt % of fullerene electrons are extracted in ~40 ns at a −3 V bias, whereas the hole extraction takes ~200 ns. This indicates that carrier extraction is slightly unbalanced in optimized devices. The insets show the simulated electron and hole mobilities. In the blends with the fullerene content of 60, 80, and 90 wt %, the electron mobility in the first 10 ps after the pump pulse is >0.1 $cm^2\ V^{-1}\ s^{-1}$. High electron mobility drives fast dissociation of generated charge pairs into free carriers. The blend with 90 wt % of fullerene shows a weak $\mu_e \propto t^{-0.3}$ time dependence which can be explained by electron trapping at low energy sites. For comparison, the electron mobility in blends with 60 and 80 wt % fullerene shows a stronger time dependence $\mu_e \propto t^{-0.6}$, suggesting that there is another mechanism that slows down the electron mobility in addition to relaxation to low energy sites. It is natural to assume that the electron mobility decreases when electrons reach the boundaries of fullerene clusters and fullerene-rich domains. This assumption is supported by an about 10 times lower initial electron mobility in the blend with 10 wt % fullerene and its rapid decrease with time as $\mu_e \propto t^{-0.7}$, both showing that the electron transport is at a percolation limit in this blend. The highest initial hole mobility is observed in the optimized blend with 40 wt % of polymer and not in the blend with 90 wt % of polymer, indicating that the slow dissociation of bound electron−hole pairs limits the hole mobility in the polymer-rich blend. The time-dependence of hole mobility is very similar to that of electrons and follows $\mu_h \propto t^{-0.3}$ in the polymer-rich blend, which changes to $\mu_h \propto t^{-0.7}$ in the blend with 10 wt % of the polymer. Our results suggest comparable hole and electron mobilities of around 10^{-4} $cm^2\ V^{-1}\ s^{-1}$ in the blends with 60 wt % fullerene at 100 ns. This is in good agreement with the previously reported electron and hole mobilities for space-charge-limited current in blends of PTB7 with the fullerene $PC_{61}BM$ with the same blend ratio.[24] The same study has reported a sharp decrease of hole mobility when the fullerene concentration increased beyond 83 wt %, which also agrees with our results. This suggests that approximation of the time-dependent carrier mobility using the power law functions give a realistic separation of the integrated electron and hole photocurrents. Our results also suggest that the mobility of both types of carriers is controlled by low energy and spatial traps in the blends. The initial values of hole mobility, however, are not strongly dependent on the blend ratio. This can be explained by the faster hole transport along the conjugated polymer chains as compared to transport between chains.[25]

DISCUSSION

Let us discuss our experimental findings by taking into consideration the results of previous studies of blend morphology and the influence of the solvent additive. In the most efficient blend of [P40:F60] with DIO, an optimum morphology of a finely interpenetrating network of PTB7 and $PC_{71}BM$ is formed and the total amount of extracted charge is double that of a blend prepared without DIO. Here, we have been able to show that this enhancement is based on a higher dissociation efficiency of generated charge pairs into free carriers which is independent of the applied electric field. An internal quantum efficiency of >0.9 has been demonstrated in PTB7:$PC_{71}BM$ solar cells prepared with DIO,[4−6,12] implying that the free carrier generation efficiency is close to unity in optimized blends. Since the charge-generation efficiency was found to be similar in blends prepared with additive and without,[12] this indicates that about a half of generated charge pairs in the blends prepared without DIO never dissociate into free charge carriers. Previous studies of morphology and photophysics of PTB7:$PC_{71}BM$ blends prepared without additive showed large pure fullerene clusters of 20−60 nm in size which were embedded in a polymer-rich phase with about 30 wt % of fullerene mixed in it.[10−13] Based on our observations of the pair dissociation efficiency being low in polymer-rich blends, we suggest that the geminate charge pairs generated between polymer and dispersed fullerene molecules in the polymer-rich phase never dissociate, as illustrated in Figure 6. This happens because the hole mobility in PTB7 is inherently low and fullerene molecules in the polymer-rich phase are too far from each other. PTB7:$PC_{71}BM$ blends prepared using the additive DIO have been shown to consist of interpenetrating polymer-rich and fullerene-rich domains of tens of nanometers in size, and large pure domains were no longer observed.[10−12] These polymer- and fullerene-rich domains imply that there is a concentration gradient of donor and acceptor molecules between these domains. In such a morphology, charge separation can be thermodynamically

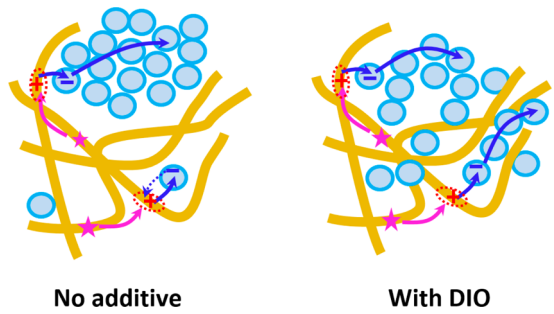

Figure 6. Schematic of the proposed charge separation mechanism in PTB7:$PC_{71}BM$ solar cells. According to previous morphology studies, the blends prepared without additive form pure fullerene clusters of 20−60 nm in size which are embedded in a polymer-rich phase with about 30 wt % fullerene mixed in it.[10−13] The charge pairs generated at the dispersed fullerene molecules do not dissociate because of low hole mobility, and only charge pairs generated at the fullerene clusters give photovoltaic response. The addition of DIO to the casting solvent improves the miscibility of $PC_{71}BM$ with PTB7 and forms interpenetrating polymer-rich and fullerene-rich phases of tens of nanometers in size.[10,12] Charge separation in these blends is driven by fast electron motion in the fullerene-rich phase. Small-scale phase separation also improves charge transport at low built-in field.

DOI: 10.1021/acs.jpcc.6b01548
J. Phys. Chem. C 2016, 120, 9588−9594

driven as the entropy increases with carrier motion from the lower to higher concentration of acceptor molecules. For efficient charge separation all fullerene molecules have to be well connected to provide unperturbed electron motion. An insight into the development of a well-connected fullerene network in blends of PTB7 with a fullerene $PC_{61}BM$ processed with DIO has been given by in situ measurements of the grazing incidence small-angle X-ray scattering during solvent evaporation.[26] These studies showed rapid formation of crystalline PTB7 aggregates driven by rapid evaporation of chlorobenzene but spontaneous phase separation was not observed presumably because of very slow evaporation of DIO which is a good solvent for fullerene molecules. Shrinkage of the fullerene domains in PTB7:fullerene blends with addition of DIO is different from DIO's role in altering the morphology in other photovoltaic blends where it promotes phase separation of two intimately mixed materials.[27] Morphology optimization increases the free carrier yield, the short circuit current and the fill factor, whereas the open circuit voltage (V_{OC}) is not affected by it (Figure 1). These results are consistent with previous observations.[5,10,12] The contacts in these cells are nonselective (no charge blocking layers); therefore, V_{OC} is determined not only by the built-in potential and charge transport but is also reduced by surface recombination (extraction to wrong contacts by diffusion). We speculate that in our case the voltage loss to surface recombination is entirely determined by contacts which can explain why V_{OC} is not different.

The increase of free carrier yield with DIO is also observed in blends with 80 and 90 wt % fullerene, but the effect is less pronounced presumably because the fullerene molecules are better connected at higher concentration even without DIO. We also found that DIO increases the carrier extraction velocity at weak electric field which can be explained by improved connectivity of nanostructured polymer-rich and fullerene-rich domains providing faster percolation channels for extraction of both types of carriers. The DIO enhances the performance of all fullerene-rich blends, but it reduces the amount of extracted charge from the polymer-rich blend. Even though the charge separation in the polymer-rich blend shows strong electric field dependence, the reduction factor of extracted charge with DIO is field-independent, suggesting that DIO changes the morphology of this nonoptimum polymer-rich blend, too.

CONCLUSIONS

Transient photocurrent and ultrafast optical measurements of carrier drift enabled us to measure charge-separation dynamics and electron and hole extraction in PTB7:$PC_{71}BM$ solar cells with different blend ratios. We find that the short circuit current is determined by the separation of charge pairs into free carriers. This separation is found to be efficient in fullerene-rich blends and inefficient in the polymer-rich blends, suggesting that high mobility of one type of carriers is essential for efficient charge separation. The free carrier yield is higher by a factor of 2 in devices prepared with DIO than without at the optimal blend ratio. Half of the generated charge pairs in the blends prepared without DIO never dissociate into free charge carriers, which we attribute to charge pairs generated in the polymer-rich domains with molecularly dispersed fullerene molecules. DIO only weakly influences the carrier mobility. The carrier extraction rate slightly increases with morphology optimization with DIO, but only at a low built-in electric fields. These findings explain the higher photocurrent and fill factor of devices prepared with DIO. Our results also show that carrier extraction is unbalanced in optimized devices with electron extraction being about 10 times faster than the hole extraction.

AUTHOR INFORMATION

Corresponding Authors

*E-mail: idws@st-andrews.ac.uk. Tel: +44 (0)1334 463114.
*E-mail: vidmantas.gulbinas@ftmc.lt. Tel: +370 62125615.

Author Contributions

The manuscript was written through contributions of all authors. All authors have given approval to the final version of the manuscript.

Notes

The authors declare no competing financial interest.

ACKNOWLEDGMENTS

This work was supported by the Research Council of Lithuania (Project No. MIP-85/2015), the Engineering and Physical Sciences Research Council of the UK (Grant Nos. EP/J009016/1 and EP/L012294/1), and the European Research Council of the European Union (Grant No. 321305). I.D.W.S. also acknowledges support from a Royal Society Wolfson Research Merit Award. D.A.V. is grateful to Supergen SuperSolar Hub for the travel grant. The research data supporting this publication can be accessed at http://dx.doi.org/10.17630/530a6c5a-fdb4-4944-af17-855d2b90e29b.

REFERENCES

(1) Chen, J.; Cui, C.; Li, Y.; Zhou, L.; Ou, Q.; Li, C.; Li, Y.; Tang, J.-X. Single-Junction Polymer Solar Cells Exceeding 10% Power Conversion Effi Ciency. *Adv. Mater.* **2015**, *27*, 1035−1041.
(2) Liu, Y.; Zhao, J.; Li, Z.; Mu, C.; Ma, W.; Hu, H.; Jiang, K.; Lin, H.; Ade, H.; Yan, H. Aggregation and Morphology Control Enables Multiple Cases of High-Efficiency Polymer Solar Cells. *Nat. Commun.* **2014**, *5*, 5293.
(3) He, Z.; Xiao, B.; Liu, F.; Wu, H.; Yang, Y.; Xiao, S.; Wang, C.; Russell, T. P.; Cao, Y. Single-Junction Polymer Solar Cells with High Efficiency and Photovoltage. *Nat. Photonics* **2015**, *9*, 174−179.
(4) Ouyang, X.; Peng, R.; Ai, L.; Zhang, X.; Ge, Z. Efficient Polymer Solar Cells Employing a Non-Conjugated Small-Molecule Electrolyte. *Nat. Photonics* **2015**, *9*, 520−524.
(5) Liang, Y.; Xu, Z.; Xia, J.; Tsai, S. T.; Wu, Y.; Li, G.; Ray, C.; Yu, L. For the Bright Future-Bulk Heterojunction Polymer Solar Cells with Power Conversion Efficiency of 7.4%. *Adv. Mater.* **2010**, *22*, E135−E138.
(6) He, Z.; Zhong, C.; Su, S.; Xu, M.; Wu, H.; Cao, Y. Enhanced Power-Conversion Efficiency in Polymer Solar Cells Using an Inverted Device Structure. *Nat. Photonics* **2012**, *6*, 593−597.
(7) Yao, Y.; Hou, J.; Xu, Z.; Li, G.; Yang, Y. Effects of Solvent Mixtures on the Nanoscale Phase Separation in Polymer Solar Cells. *Adv. Funct. Mater.* **2008**, *18*, 1783−1789.
(8) Zhang, F.; Jespersen, K. G.; Björström, C.; Svensson, M.; Andersson, M. R.; Sundström, V.; Magnusson, K.; Moons, E.; Yartsev, a.; Inganäs, O. Influence of Solvent Mixing on the Morphology and Performance of Solar Cells Based on Polyfluorene Copolymer/Fullerene Blends. *Adv. Funct. Mater.* **2006**, *16*, 667−674.
(9) Lee, J. K.; Ma, W. L.; Brabec, C. J.; Yuen, J.; Moon, J. S.; Kim, J. Y.; Lee, K.; Bazan, G. C.; Heeger, A. J. Processing Additives for Improved Efficiency from Bulk Heterojunction Solar Cells. *J. Am. Chem. Soc.* **2008**, *130*, 3619−3623.
(10) Collins, B. A.; Li, Z.; Tumbleston, J. R.; Gann, E.; McNeill, C. R.; Ade, H. Absolute Measurement of Domain Composition and Nanoscale Size Distribution Explains Performance in PTB7:PC 71 BM Solar Cells. *Adv. Energy Mater.* **2013**, *3*, 65−74.
(11) Hammond, M. R.; Kline, R. J.; Herzing, A. a; Richter, L. J.; Germack, D. S.; Ro, H.; Soles, C. L.; Fischer, D. a; Xu, T.; Yu, L.; et al.

DOI: 10.1021/acs.jpcc.6b01548
J. Phys. Chem. C 2016, 120, 9588−9594

Molecular Order in High-Efficiency Polymer/Fullerene Bulk Heterojunction Solar Cells. *ACS Nano* **2011**, *5*, 8248−8257.
(12) Hedley, G. J.; Ward, A. J.; Alekseev, A.; Howells, C. T.; Martins, E. R.; Serrano, L. a; Cooke, G.; Ruseckas, A.; Samuel, I. D. W. Determining the Optimum Morphology in High-Performance Polymer-Fullerene Organic Photovoltaic Cells. *Nat. Commun.* **2013**, *4*, 2867.
(13) Lou, S. J.; Szarko, J. M.; Xu, T.; Yu, L.; Marks, T. J.; Chen, L. X. Effects of Additives on the Morphology of Solution Phase Aggregates Formed by Active Layer Components of High-Efficiency Organic Solar Cells. *J. Am. Chem. Soc.* **2011**, *133*, 20661−20663.
(14) Yao, E.-P.; Chen, C.-C.; Gao, J.; Liu, Y.; Chen, Q.; Cai, M.; Hsu, W.-C.; Hong, Z.; Li, G.; Yang, Y. The Study of Solvent Additive Effects in Efficient Polymer Photovoltaics via Impedance Spectroscopy. *Sol. Energy Mater. Sol. Cells* **2014**, *130*, 20−26.
(15) Wang, Z.; Zhang, F.; Li, L.; An, Q.; Wang, J.; Zhang, J. The Underlying Reason of DIO Additive on the Improvement Polymer Solar Cells Performance. *Appl. Surf. Sci.* **2014**, *305*, 221−226.
(16) Chang, S.-Y.; Liao, H.-C.; Shao, Y.-T.; Sung, Y.-M.; Hsu, S.-H.; Ho, C.-C.; Su, W.-F.; Chen, Y.-F. Enhancing the Efficiency of Low Bandgap Conducting Polymer Bulk Heterojunction Solar Cells Using P3HT as a Morphology Control Agent. *J. Mater. Chem. A* **2013**, *1*, 2447−2452.
(17) Devižis, A.; Serbenta, A.; Meerholz, K.; Hertel, D.; Gulbinas, V. Ultrafast Dynamics of Carrier Mobility in a Conjugated Polymer Probed at Molecular and Microscopic Length Scales. *Phys. Rev. Lett.* **2009**, *103*, 027404.
(18) Pranculis, V.; Infahsaeng, Y.; Tang, Z.; Devižis, A.; Vithanage, D. A.; Ponseca, C. S.; Inganäs, O.; Yartsev, A. P.; Gulbinas, V.; Sundström, V. Charge Carrier Generation and Transport in Different Stoichiometry APFO3:PC61BM Solar Cells. *J. Am. Chem. Soc.* **2014**, *136*, 11331−11338.
(19) Gelinas, S.; Rao, A.; Kumar, A.; Smith, S. L.; Chin, A. W.; Clark, J.; van der Poll, T. S.; Bazan, G. C.; Friend, R. H. Ultrafast Long-Range Charge Separation in Organic Semiconductor Photovoltaic Diodes. *Science (Washington, DC, U. S.)* **2014**, *343*, 512−516.
(20) Lane, P. A.; Cunningham, P. D.; Melinger, J. S.; Esenturk, O.; Heilweil, E. J. Hot Photocarrier Dynamics in Organic Solar Cells. *Nat. Commun.* **2015**, *6*, 7558.
(21) Burkhard, G. F.; Hoke, E. T.; Beiley, Z. M.; Mcgehee, M. D. Free Carrier Generation in Fullerene Acceptors and Its Effect on Polymer Photovoltaics. *J. Phys. Chem. C* **2012**, *116*, 26674−26678.
(22) Devižis, A.; Hertel, D.; Meerholz, K.; Gulbinas, V.; Moser, J.-E. Time-Independent, High Electron Mobility in Thin PC61BM Films: Relevance to Organic Photovoltaics. *Org. Electron.* **2014**, *15*, 3729−3734.
(23) Bartelt, J. A.; Beiley, Z. M.; Hoke, E. T.; Mateker, W. R.; Douglas, J. D.; Collins, B. a.; Tumbleston, J. R.; Graham, K. R.; Amassian, A.; Ade, H.; et al. The Importance of Fullerene Percolation in the Mixed Regions of Polymer-Fullerene Bulk Heterojunction Solar Cells. *Adv. Energy Mater.* **2013**, *3*, 364−374.
(24) Foster, S.; Deledalle, F.; Mitani, A.; Kimura, T.; Kim, K.-B.; Okachi, T.; Kirchartz, T.; Oguma, J.; Miyake, K.; Durrant, J. R.; et al. Electron Collection as a Limit to Polymer:PCBM Solar Cell Efficiency: Effect of Blend Microstructure on Carrier Mobility and Device Performance in PTB7:PCBM. *Adv. Energy Mater.* **2014**, *4*, 1400311.
(25) Devižis, A.; Meerholz, K.; Hertel, D.; Gulbinas, V. Hierarchical Charge Carrier Motion in Conjugated Polymers. *Chem. Phys. Lett.* **2010**, *498*, 302−306.
(26) Liu, F.; Zhao, W.; Tumbleston, J. R.; Wang, C.; Gu, Y.; Wang, D.; Briseno, A. L.; Ade, H.; Russell, T. P. Understanding the Morphology of PTB7:PCBM Blends in Organic Photovoltaics. *Adv. Energy Mater.* **2014**, *4*, 1−9.
(27) Albrecht, S.; Schindler, W.; Kurpiers, J.; Kniepert, J.; Blakesley, J. C.; Dumsch, I.; Allard, S.; Fostiropoulos, K.; Scherf, U.; Neher, D. On the Field Dependence of Free Charge Carrier Generation and Recombination in Blends of PCPDTBT/PC70BM: Influence of Solvent Additives. *J. Phys. Chem. Lett.* **2012**, *3*, 640−645.

DOI: 10.1021/acs.jpcc.6b01548
J. Phys. Chem. C 2016, 120, 9588−9594